

Graph Neural Networks for modelling breast biomechanical compression

Hadeel Awwad^[0009–0007–4054–4546], Eloy García^[0000–0002–0587–1919], and Robert Martí^[0000–0002–8080–2710]

Computer Vision and Robotics Institute, University of Girona, Girona, Spain
{`robert.marti`}@udg.edu

Abstract. Breast compression simulation is essential for accurate image registration from 3D modalities to X-ray procedures like mammography. It accounts for tissue shape and position changes due to compression, ensuring precise alignment and improved analysis. Although Finite Element Analysis (FEA) is reliable for approximating soft tissue deformation, it struggles with balancing accuracy and computational efficiency. Recent studies have used data-driven models trained on FEA results to speed up tissue deformation predictions. We propose to explore Physics-based Graph Neural Networks (PhysGNN) for breast compression simulation. PhysGNN has been used for data-driven modelling in other domains, and this work presents the first investigation of their potential in predicting breast deformation during mammographic compression. Unlike conventional data-driven models, PhysGNN, which incorporates mesh structural information and enables inductive learning on unstructured grids, is well-suited for capturing complex breast tissue geometries. Trained on deformations from incremental FEA simulations, PhysGNN’s performance is evaluated by comparing predicted nodal displacements with those from finite element (FE) simulations. This deep learning (DL) framework shows promise for accurate, rapid breast deformation approximations, offering enhanced computational efficiency for real-world scenarios.

Keywords: Breast computed tomography · Digital breast phantom · Multimodal imaging fusion · 2D-3D image registration · Mammography · Finite element models

1 Introduction

Breast cancer is one of the most prevalent and, life-threatening cancers affecting women worldwide. The high incidence rate underscores the critical need for early and accurate diagnosis to improve patient outcomes [19,25]. Common diagnostic modalities include mammography, magnetic resonance imaging (MRI), ultrasound, and dedicated breast computed tomography (BCT), each offering unique benefits in detecting and characterizing breast lesions [2,20,23,24]. Integrating and correlating information from these diverse imaging techniques can significantly enhance diagnostic accuracy. By synthesizing and simulating data

from 3D modalities like MRI and BCT into 2D representations as seen in mammography, clinicians can leverage the comprehensive structural details of MRI or BCT with the practical format of mammography. This multi-modal strategy provides a more comprehensive perspective of breast tissue, enhancing lesion detection and assessment, and ultimately improving diagnostic outcomes and patient care.

Achieving realistic breast compression simulation is crucial for multi-modal breast imaging correspondence, commonly approached using Finite Element Analysis (FEA) methods. However, the limited computational efficiency of FEA poses a significant challenge in medical image registration, as it requires substantial time and resources to solve biomechanical models accurately. This limitation affects the performance of existing multimodal registration techniques. To address this issue, researchers have proposed data-driven models that train different machine learning algorithms with FEA results to speed up tissue deformation approximations by prediction [9,10,12,13,14]. However, these methods overlook valuable information contained within the FE mesh structure, such as node connections and distances, and their number of parameters depends on the mesh resolution.

To the best of our knowledge, this study is the first to adapt the PhysGNN model proposed by Salehi [15] for simulating breast compression. It provides a comparative analysis of the results using both quantitative and qualitative metrics against existing FEA methods and discusses its benefits and limitations.

2 Materials

BCT is an advanced imaging modality that provides high-resolution, three-dimensional breast images, offering superior tissue contrast compared to digital mammography, see Figure 1 (a). This enhanced imaging capability facilitates better detection and characterization of breast lesions. This work used a publicly available dataset of computational digital phantoms generated from clinical BCT images previously obtained at UC Davis (California, USA) [1,7,16], utilizing a semi-automatic tissue classification algorithm [11]. Each voxel of the breast phantom was segmented into various classes: air, fatty tissue, glandular tissue, and skin tissue. In this work, we have used a single phantom (Uncompressed-Breast3) for generating the geometry of the biomechanical model. We chose to use a single phantom because generating incremental FEA solutions is computationally expensive. Future research can explore additional breast phantoms to test PhysGNN’s capability in predicting the deformation of various geometries.

3 Methods

Figure 1 (b) outlines the workflow of the proposed method to approximate mammographic compression using a biomechanical breast model to train the PhysGNN model, detailed in the following sections.

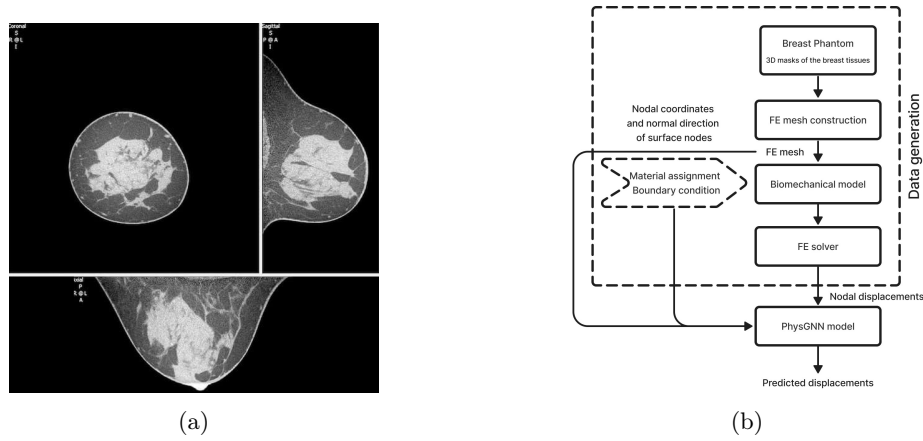


Fig. 1: (a) Reconstructed dataset from breast CT [7]. (b) Flow chart of the proposed method to simulate the breast compression using PhysGNN.

3.1 Biomechanical Breast Model

The breast biomechanical model is derived from García’s work [5]. An overview of generating a biomechanical breast model is shown in Figure 2 involving breast geometry and mesh generation, material properties and boundary conditions definition, and the finite element solver.

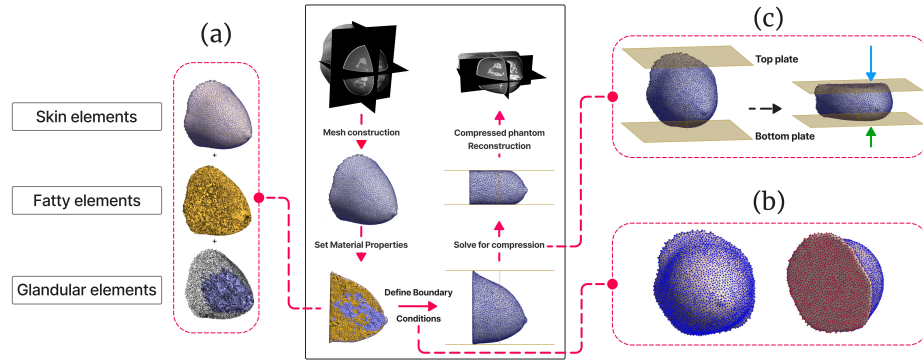


Fig. 2: Overview of steps to set up and solve compressed breast geometry using FEA, then apply deformation to reposition and compress the breast phantom.

Generation of the Finite Element Mesh To represent the breast geometry, we used a meshing technique that discretizes the breast volume into small tetrahedral elements [18]. These elements form a graph-like structure, approximating the breast’s complex geometry with tetrahedrons, each having four

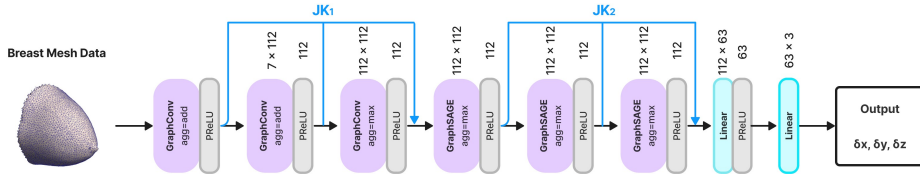


Fig. 3: Architectural diagram of PhysGNN [15]

triangular faces and four nodes. The FE volume mesh for running FE simulations was generated by running Pygalmesh [17], a Python interface to the CGAL library [21] to generate high-quality 3D volume mesh. Figure 2 (a) illustrates the FE volume mesh of the breast phantom, which consists of 17595 nodes and 95865 tetrahedral elements. More details on the FE volume mesh may be found in Table 3, Appendix 1.

Material Properties and Boundary Conditions The material behaviour of breast tissues was characterized as nearly incompressible, with a Poisson ratio of 0.49, using homogeneous and isotropic Neo-Hookean material models as reported in the literature [22]. The stiffness measures were assigned using Young’s modulus ($E_{\text{fatty}} = 4.46 \text{ kPa}$, $E_{\text{glandular}} = 15.1 \text{ kPa}$, $E_{\text{skin}} = 20.0 \text{ kPa}$). The boundary condition was set to restrict rigid motion by constraining the posterior surface of the breast in the anterior-posterior direction. See Figure 2 (b), which is colour-coded by boundary conditions: free nodes (blue) throughout the breast and constrained nodes (red) on the posterior surface to mimic chest wall restriction.

Finite Element Simulations While FEA is a common method for solving the compression, this work specifically focuses on simulating compression for the Cranio Caudal (CC) view during mammography. The results from FEA simulations are utilized as ground truth to train the PhysGNN model in predicting breast compression, see next section. NiftySim (v.2.3.1; University College London, UK) [8] is used to conduct incremental FE simulations on the FE mesh, modelled using two frictionless infinite linear planes [5], see Figure 2 (c).

3.2 PhysGNN

In this work, we explore PhysGNN proposed by Salehi [15], which approximates soft tissue deformation under prescribed forces by leveraging Graph Neural Networks (GNN)s. Figure 3 illustrates the architecture of PhysGNN, integrating GraphSAGE and GraphConv layers with Jumping Knowledge (JK) connections. This design facilitates inductive learning over graphs through *parameter sharing*, ensuring a constant number of parameters regardless of the mesh size. This approach enhances computational feasibility when learning from high-quality meshes with numerous nodes [15].

A training and testing dataset was generated from the incremental simulations of NiftySim by applying a force of 90 Newtons to the breast surface nodes, incrementally over 30-time steps and in 40 directions, to capture the non-linear

behaviour of soft tissue under large forces. The forces applied to each surface node are directed along its surface normal (x , y , and z) and three additional randomly sampled directions. Each additional direction is represented as a tuple (x , y , and z) randomly selected from a unit-radius hemisphere. Note that this is slightly different from the original implementation of [15] where only 10 distinct batches of random directions were included, along with the surface normal direction. Further details on the generated dataset can be found in Table 4, Appendix 2.

The input features for PhysGNN include force values applied to surface nodes in Cartesian coordinates (F_x, F_y, F_z) and spherical coordinates (F_ρ, F_θ, F_ϕ). Each node is also assigned a Physical Property value: 0.1 for skin, 0.6 for glandular tissue, 1 for fatty tissue under free boundary conditions, and 0 for fixed boundary conditions. This value impacts the node’s displacement, influenced by its boundary condition and Young’s modulus. Fatty tissue tends to experience larger displacements due to its smaller Young’s modulus compared to glandular and skin tissues. PhysGNN outputs displacement values ($\delta_x, \delta_y, \delta_z$) for the mesh nodes. Edge weights ($e_{u,v}$) in the GNN model are computed as the inverse of the Euclidean distance between adjacent nodes u and v , with $u, v \in \mathcal{N}$. Information about PhysGNN hyperparameters and infrastructure settings can be found in Appendix 3.

3.3 Voxelised Compressed Phantom Reconstruction

Predicted deformations by FEA and PhysGNN are used to reconstruct the compressed voxel phantom following the method in [3,6]. The compressed FE mesh is converted into a voxelized phantom, with elements stored on a uniform grid. Each voxel’s position is mapped to the uncompressed model using barycentric coordinates [3]. This transforms points along a ray in the compressed model to a curve in the segmented BCT image, with labels obtained using nearest neighbour interpolation.

3.4 PhysGNN Training Experiments

We evaluate the performance of PhysGNN model on Hold-out and Leave-one-deformation-out (LODO) strategies against the results of FEA (our baseline).

Hold-out experiment The dataset from step-wise compression of a single BCT phantom obtained using FEA NiftySim was randomly split into training (70%), validation (20%), and testing (10%) sets. Despite using a single breast phantom with 30 deformation states, this experiment provides valuable groundwork for future studies involving additional breast models.

Leave-one-deformation-out experiment To evaluate the model’s ability to generalize to unseen deformations, a specific testing strategy was used. From 30 NiftySim-simulated deformations, one (the final compression state) was isolated for testing. The remaining 29 were split into training (80%) and validation (20%) sets. This approach reflects real-world scenarios where models train on

known deformations and predict new ones for a complete breast geometry. Note that the training data is from a single BCT phantom.

3.5 Evaluation Metrics

Similar to previous research [9,14], the PhysGNN model predictions are evaluated against FEA results, which serve as the ground truth. We use several evaluation metrics to assess model performance and accuracy. The Dice coefficient measures the agreement between segmented images. The Mean Euclidean Error (MEE) and Mean Absolute Error (MAE) assess prediction accuracy based on node positions, with MEE measuring the average distance between predicted and ground truth positions, and MAE evaluating the average error magnitude of node displacements. Lastly, the Volume Loss metric measures the difference in breast tissue volume before and after compression, reflecting the physical realism and accuracy of the biomechanical models. These metrics collectively provide a comprehensive assessment of the model’s performance.

4 Results and Discussion

4.1 Performance of PhysGNN Model

Table 1 shows PhysGNN’s performance in predicting breast deformation under mammographic compression. PhysGNN effectively predicts deformations, with 99.96% of nodal position errors under 1 mm in the Hold-out experiment and 81.22% in the LODO experiment. The Hold-out evaluation offers more stable performance estimates than LODO, which is computationally expensive and limits model complexity and hyperparameter tuning. Additionally, single-deformation testing in LODO may not accurately reflect performance on diverse deformations. Table 5 in Appendix 4 presents the PhysGNN test set statistics.

Table 1: The performance of PhysGNN model on Hold-out and Leave-one-deformation-out on the test set. Exp. stands for Experiment

Exp.	MAE (δx) (mm)	MAE (δy) (mm)	MAE (δz) (mm)	Mean Euclidean Error (mm)	Euclidean Error \leq 1 mm (%)	Mean Absolute Position Error (mm)	Absolute Position Error \leq 1 mm (%)
Hold-out	0.17 ± 0.18	0.20 ± 0.20	0.13 ± 0.14	0.34 ± 0.15	97.50	0.17 ± 0.03	99.96
LODO	0.56 ± 0.44	0.52 ± 0.39	0.67 ± 0.52	1.21 ± 0.44	33.51	0.59 ± 0.07	81.22

In the Hold-out experiment, predicting tissue deformation took 0.42 ± 0.04 seconds on CPU and 0.01 ± 0.06 seconds on GPU. In the LODO experiment, it took 0.82 seconds on CPU and 0.47 seconds on GPU. Incremental NiftySim simulations, with GPU acceleration, totalled 4640.5 seconds (154.7 seconds per simulation). This indicates a speedup of 329 times with GPU and 188 times with CPU in the LODO experiment compared to a single NiftySim simulation.

4.2 Quantitative and Qualitative Analysis of Leave-one-deformation-out experiment

We present here additional quantitative and qualitative results only for the LODO experiment. For the Hold-out experiment, since graphs from different deformations are mixed in the test set, a specific evaluation cannot be provided.

Figure 4 compares the reconstructed phantoms from PhysGNN-predicted deformation using the LODO strategy to the final compression state by NiftySim, which serves as the ground truth. The results show that PhysGNN closely matches FEA in breast deformation predictions, demonstrating its effectiveness and potential as a reliable alternative to traditional FEA methods. The similarity is further quantified by the Dice scores: 0.94 for fat tissue, 0.83 for glandular tissue, and 0.53 for skin tissue, indicating high values for primary tissues (excluding skin, which is very thin and thus results in a compromised Dice score).

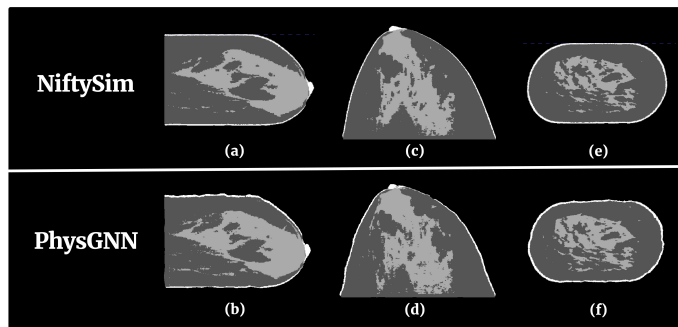


Fig. 4: Cross-sectional views of compressed digital phantoms from NiftySim and PhysGNN: (a) and (b) sagittal sections, (c) and (d) axial sections, (e) and (f) coronal sections

Finally, Table 2 summarizes the volume loss percentages for total breast, fatty, glandular, and skin tissues. PhysGNN predictions show a slightly increased overall breast tissue loss.

We can also visually assess the displacement magnitudes on the BCT model with each method as shown in Figure 5. Figure 5 (a) shows NiftySim’s displacements, Figure 5 (b) shows PhysGNN’s predicted displacements, and Figure 5 (c)

Table 2: Breast tissue loss during compression

FEA/DL	Total breast volume loss(%)	Fatty tissue volume loss(%)	Glandular tissue volume loss(%)	Skin tissue volume loss(%)
NiftySim	1.03	0.38	0.03	10.33
PhysGNN	1.26	0.55	0.34	10.94

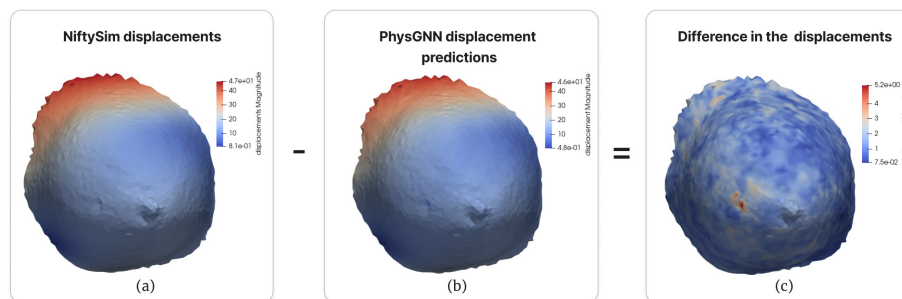


Fig. 5: Output displacements (mm) of NiftySim and PhysGNN on the FE model

highlights the differences. While overall patterns are similar, noticeable dissimilarity exists on the breast surface, with a maximum displacement difference of 5.2 mm.

The overall results show strong performance with low errors and visual similarity to the NiftySim ground truth, suggesting the model is nearing practical applicability. However, the necessity for training on incremental FEA simulations, which requires significant training time, remains a challenge. Despite this, the method holds promise for multiple compression simulations, particularly within an optimization framework for 2D/3D registration, as demonstrated by García’s work [4]. Thus, PhysGNN has significant potential for specialized scenarios requiring detailed and repeated simulations.

5 Conclusion

This work is the first to apply GNNs for predicting breast deformation during mammographic compression, comparing quantitatively and qualitatively with standard FEA models. The PhysGNN model, trained on FEA displacement data, achieved a Mean Euclidean Error of 0.34 ± 0.15 mm in the Hold-out experiment. The PhysGNN model achieved accurate results comparable to the FEA, with a speedup of factor 329 and 188 using GPU and CPU, respectively in the Leave-one-deformation-out experiment, suggesting its potential to replace FEA simulations for real-time clinical applications. For future work, it is important to include simulations of compression for the Mediolateral Oblique (MLO) view during mammography. Further efforts should focus on comparing PhysGNN with other FEA methods to assess relative performance. Additionally, the study

should be extended to generalize the model to multiple geometries, examining its robustness and accuracy across diverse scenarios. Finally, integrating PhysGNN into 2D/3D registration frameworks could further enhance its applicability and effectiveness in clinical settings.

Acknowledgments. This work has been partially funded by the Erasmus+ Erasmus Mundus Joint Master’s Degree (EMJMD) scholarship (2022–2024), with project reference 610600-EPP-1-2019-1-ES-EPPKA1-JMD-MOB and the project VICTORIA, “PID2021-123390OB-C21” from the Ministerio de Ciencia e Innovación of Spain.

Disclosure of Interests. The authors have no competing interests to declare relevant to this article’s content.

References

1. Boone, J.M., Nelson, T.R., Lindfors, K.K., Seibert, J.A.: Dedicated breast ct: Radiation dose and image quality evaluation. *Radiology* **221**(3), 657–667 (2001)
2. Caballo, M., Pangallo, D.R., Sanderink, W., Hernandez, A.M., Lyu, S.H., Molinari, F., Boone, J.M., Mann, R.M., Sechopoulos, I.: Multi-marker quantitative radiomics for mass characterization in dedicated breast ct imaging. *Medical Physics* (2021)
3. García, E., Diez, Y., Diaz, O., Lladó, X., Gubern-Mérida, A., Martí, R., Martí, J., Oliver, A.: Multimodal breast parenchymal patterns correlation using a patient-specific biomechanical model. *IEEE Transactions on Medical Imaging* **37**(3), 712–723 (2018)
4. García, E., Diez, Y., Diaz, O., Lladó, X., Gubern-Mérida, A., Martí, R., Martí, J., Oliver, A.: Breast mri and x-ray mammography registration using gradient values. *Medical Image Analysis* **54**, 76–87 (2019)
5. García, E., Fedon, C., Caballo, M., Martí, R., Sechopoulos, I., Diaz, O.: Realistic compressed breast phantoms for medical physics applications. In: 15th International Workshop on Breast Imaging (IWBI2020). p. 73. SPIE (05 2020)
6. García, E., Oliver, A., Diaz, O., Diez, Y., Gubern-Mérida, A., Martí, R., Martí, J.: Mapping 3d breast lesions from full-field digital mammograms using subject-specific finite element models. In: Society of Photo-Optical Instrumentation Engineers (SPIE) Conference Series. vol. 10135, p. 1013504 (2017)
7. Gazi, P.M., Yang, K., Burkett, G. W., J., Aminololama-Shakeri, S., Seibert, J.A., Boone, J.M.: Evolution of spatial resolution in breast ct at uc davis. *Medical physics* **42**(4), 1973–1981 (2015)
8. Johnsen, S.F., Taylor, Z.A., Clarkson, M.J., et al.: Niftysim: A gpu-based nonlinear finite element package for simulation of soft tissue biomechanics. *International Journal of Computer Assisted Radiology and Surgery (Int J CARS)* **10**(7), 1077–1095 (2015)
9. Martínez-Martínez, F., Rupérez-Moreno, M., Martínez-Sober, M., Solves-Llorens, J., Lorente, D., Serrano-López, A., Martínez-Sanchis, S., Monserrat, C., Martín-Guerrero, J.: A finite element-based machine learning approach for modeling the mechanical behavior of the breast tissues under compression in real-time. *Computers in Biology and Medicine* **90**, 116–124 (2017)
10. Mendizabal, A., Tagliabue, E., Brunet, J.N., Dall’Alba, D., Fiorini, P., Cotin, S.: Physics-based deep neural network for real-time lesion tracking in ultrasound-guided breast biopsy. In: *Computational Biomechanics for Medicine: Solid and Fluid Mechanics for the Benefit of Patients* 22. pp. 33–45 (2020)

11. Mettivier, G., Sarno, A., Boone, J.M., Bliznakova, K., di Franco, F., Russo, P.: Virtual clinical trials in 3D and 2D breast imaging with digital phantoms derived from clinical breast CT scans. In: *Medical Imaging 2020: Physics of Medical Imaging*, vol. 11312, p. 1131259 (2020)
12. Phellan, R., Hachem, B., Clin, J., Mac-Thiong, J.M., Duong, L.: Real-time biomechanics using the finite element method and machine learning: Review and perspective. *Medical Physics* **48**(1), 7–18 (2021)
13. Rupérez, M., Martínez-Martínez, F., Martínez-Sober, M., Lago, M., Lorente, D., Bakic, P., Serrano-López, A., Martínez-Sanchis, S., Monserrat, C., Martín-Guerrero, J.: Modeling the mechanical behavior of the breast tissues under compression in real time. In: *VipIMAGE 2017: Proceedings of the VI ECCOMAS Thematic Conference on Computational Vision and Medical Image Processing Porto, Portugal, October 18-20, 2017*. pp. 583–592 (2018)
14. Said, S., Yang, Z., Clauser, P., Ruitter, N., Baltzer, P., Hopp, T.: Estimation of the biomechanical mammographic deformation of the breast using machine learning models. *Clinical Biomechanics* **110**, 106117 (2023)
15. Salehi, Y., Giannacopoulos, D.: Physgnn: A physics-driven graph neural network based model for predicting soft tissue deformation in image-guided neurosurgery. *Advances in Neural Information Processing Systems* **35**, 37282–37296 (2022)
16. Sarno, A., Mettivier, G., di Franco, F., Varallo, A., Bliznakova, K., Hernandez, A.M., Boone, J.M., Russo, P.: Dataset of patient-derived 3d digital breast phantoms for research in breast computed tomography (2021)
17. Schlömer, N.: pygalmesh: Python interface for CGAL's meshing tools. Zenodo (2021)
18. Shewchuk, J.: Tetrahedral mesh generation by delaunay refinement. *Proc. 14th Annu. ACM Sympos. Comput. Geom.* (1970)
19. Sung, H., Ferlay, J., Siegel, R.L., Laversanne, M., Soerjomataram, I., Jemal, A., Bray, F.: Global cancer statistics 2020: Globocan estimates of incidence and mortality worldwide for 36 cancers in 185 countries. *CA: A Cancer Journal for Clinicians* (2021)
20. Tan, T., Rodriguez-Ruiz, A., Zhang, T., Xu, L., Beets-Tan, R.G.H., Shen, Y., Karssemeijer, N., Xu, J., Mann, R.M., Bao, L.: Multi-modal artificial intelligence for the combination of automated 3d breast ultrasound and mammograms in a population of women with predominantly dense breasts. *Insights into Imaging* (2023)
21. The CGAL Project: CGAL User and Reference Manual. CGAL Editorial Board, 5.6.1 edn. (2024)
22. Wellman, P., Howe, R.D., Dalton, E., Kern, K.A.: Breast tissue stiffness in compression is correlated to histological diagnosis. *Harvard BioRobotics Laboratory Technical Report* **1** (1999)
23. Zhang, T., Han, L., Gao, Y., Wang, X., Beets-Tan, R., Mann, R.M.: Predicting molecular subtypes of breast cancer using multimodal deep learning and incorporation of the attention mechanism. In: *Medical Imaging with Deep Learning* (2021)
24. Zhang, T., Tan, T., Han, L., Appelman, L., Veltman, J., Wessels, R., Duvivier, K.M., Loo, C., Gao, Y., Wang, X., Horlings, H.M., Beets-Tan, R.G.H., Mann, R.M.: Predicting breast cancer types on and beyond molecular level in a multi-modal fashion. *npj Breast Cancer* **9**(1), 16 (2023)
25. Zhang, T., Tan, T., Samperna, R., Li, Z., Gao, Y., Wang, X., Han, L., Yu, Q., Beets-Tan, R.G.H., Mann, R.M.: Radiomics and artificial intelligence in breast imaging: a survey. *Artificial Intelligence Review* **56**(1), 857–892 (2023)

Appendix 1

Table 3 provides information on the finite element (FE) volume mesh that was used for generating the dataset.

Table 3: Finite element volume mesh statistics

Attribute	Value
Mesh points	17595
Mesh tetrahedra	95865
Mesh triangular faces	33594
Mesh faces on the exterior surface	2300

Appendix 2

Further details on the generated training and testing datasets can be found in Table 4.

Table 4: Characteristics of the Dataset. B.C. stands for Boundary Condition

No. Fixed B.C. Nodes	No. Free B.C. Surface Nodes	No. Force magnitudes	Max. Force Applied (N)	No. Directions	No. Simulations
1171	1129	30	90	40	1200

Appendix 3

PhysGNN Hyperparameters The loss function used for learning the trainable parameters is the mean Euclidean error computed as:

$$MEE = \frac{1}{\mathcal{N}} \sum_{n \in \mathcal{N}} \sqrt{\sum_{i=1}^3 (y_n^i - \hat{y}_n^i)^2} \quad (1)$$

where \mathcal{N} is the number of mesh nodes, $\mathbf{y} \in \mathbb{R}^{\mathcal{N} \times 3}$ represents the FEM-approximated displacement in the x , y , and z directions, and $\hat{\mathbf{y}} \in \mathbb{R}^{\mathcal{N} \times 3}$ represents the displacement predicted by PhysGNN. The AdamW optimizer, with an initial learning rate of 0.005, was used to minimize the loss value, reducing the rate by a factor of 0.1 to a minimum of 1×10^{-8} if validation loss did not

improve after 5 epochs. Early stopping, halting training after 15 epochs without validation loss improvement, was employed to prevent overfitting. Additionally, a dropout rate of 0.1 was applied to the penultimate layer of PhysGNN to enhance generalization. The model was trained in 8 batches for faster convergence. **Infrastructure Settings** The FE simulations and PhysGNN model training in our study were carried out on an NVIDIA GeForce RTX 2080 Ti GPU with 46 GB.

Appendix 4

Table 5 presents the PhysGNN test set statistics of Hold-out and Leave-one-deformation-out experiments.

Table 5: The test set statistics of Hold-out and Leave-one-deformation-out, where y is the displacement, and Max. Euclidean Error_{mean} is computed as the average of the maximum Euclidean error observed for each data element—i.e., each simulation.

Experiment	δy_{\max} (mm)	δy_{mean} (mm)	Max. Euclidean Error _{mean} (mm)
Hold-out	46.56	24.02 ± 13.27	2.60 ± 1.40
LODO	46.56	46.56 ± 0.00	5.16 ± 0.00